Transient and steady-state analysis of electron transport in one-dimensional coupled quantum-box structures

H. Noguchi, J. P. Leburton,* and H. Sakaki
Research Center for Advanced Science and Technology, University of Tokyo, 4-6-1 Komaba, Meguro-ku, Tokyo 153, Japan
and Institute of Industrial Science, University of Tokyo, 7-22-1 Roppongi, Minato-ku, Tokyo 106, Japan
(Received 29 October 1992; revised manuscript received 21 January 1993)

We investigate electron transport in one-dimensional coupled quantum-box (1D-CQB) structures at room temperature by using an iterative technique for solving the time-dependent Boltzmann equation. The scattering rates in the mini-Brillouin zone are characterized by several large peaks reflecting the singularities of the 1D density of states and the features of the miniband structure. As a result of Bragg reflection, the momentum distribution function deviates significantly from a displaced Maxwellian, with carrier accumulation at the miniband edges. Under the condition of suppression of optic-phonon scattering, the time evolution of the distribution function, and the electron velocity under high electric field undergo damped Bloch oscillations with a period of a few picoseconds. In the steady-state analysis, we found that the carrier mobility is a strong function of the structure confinement and periodicity parameters.

I. INTRODUCTION

In the past few years, quantum microstructures[1–3] (QMS's) such as quantum wires and quantum boxes (QB's) have attracted much attention because they manifest fundamental phenomena such as quantum interferences[4] and single-electron effects.[5] The observation of these quantum effects is presently limited to very low temperatures because of the requirement of a dissipation-free environment and the difficulty of achieving a confinement dimension below 100 nm with energy-level separation in excess of a few meV. It is, however, anticipated that continuous improvement and innovation in nanostructure technology will provide new opportunities to realize QMS's with feature sizes smaller than 500 Å,[6] and expand the research activities on QMS's to high temperatures.

One of the most remarkable features of QMS's is their flexibility to geometrical confinement and design to achieve arbitrary spectra of electronic states and they provide new windows for technological innovation. Recently, Sakaki[3] proposed a nanostructure consisting of a one-dimensional chain of identically coupled QB's (1D-CQB's) [Fig. 1(a)]. This new periodic structure can be arbitrarily designed according to the confining potential and its periodicity. The dispersion relation and the density of states (DOS) are shown in Fig. 1(b). For certain values of the 1D-CQB parameters, it is possible to suppress polar optical-phonon (POP) scattering which is a dominant dissipation process at room temperature. Namely, if the miniband width ε_b is smaller than the POP energy $\hbar\omega_{\mathrm{POP}}$ (=36 meV in GaAs), intraminiband POP scattering does not occur. Furthermore, if the minigap width ε_g exceeds $\hbar\omega_{\mathrm{POP}}$, interminiband scattering is also prohibited. This condition is expressed as

$$\varepsilon_b < \hbar\omega_{\mathrm{POP}} , \quad \varepsilon_g > \hbar\omega_{\mathrm{POP}} . \tag{1}$$

With the suppression of POP scattering, it is expected that the transport performance of 1D-CQB's will be significantly enhanced, even at room temperature. Moreover, strong nonparabolicity of the miniband shape, and the short periodicity of the mini-Brillouin zone, are well suited for strong nonlinear effects such as negative resistance and Bloch oscillations.[7]

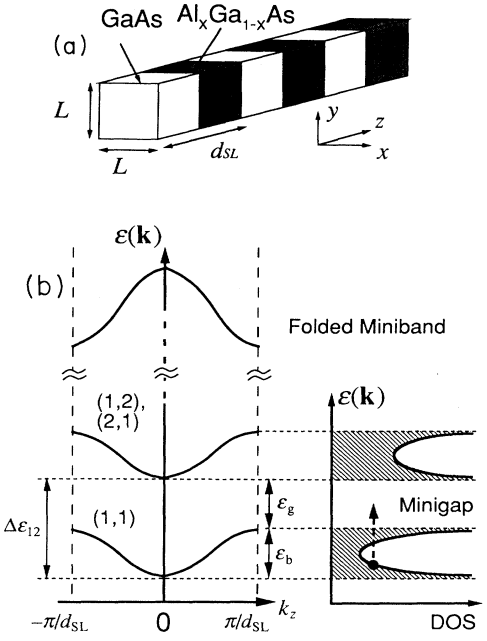

FIG. 1. (a) Schematic illustration of 1D-CQB's. (b) Dispersion relation and density of states of 1D-CQB's. Numbers on the miniband denote the index (m,n) as defined in the text. The folded miniband locates much higher than the minibands considered in the text. The dashed arrow in the DOS indicates a prohibited process of the absorption of optical phonon.

0163-1829/93/47(23)/15593(8)/$06.00

In this paper, we study electron transport in 1D-CQB structures at lattice temperature $T_L = 300$ K by using an iterative technique applied to the semiclassical Boltzmann equation. In Sec. II, we describe our electronic model, and in Sec. III we calculate the scattering rates for polar optical and acoustic deformation-potential phonons in the nanostructure. In Sec. IV, we formulate the transport theory and solve numerically the Boltzmann equation. Finally, our results on steady-state and transient transport are reported in Sec. V.

II. ELECTRONIC MODEL

In modeling the electronic properties, we assume that the 1D-CQB structure consists of a system of square GaAs QB's separated by a $Al_xGa_{1-x}As$ barrier as shown in Fig. 1(a). In this 1D system, electrons are strictly confined in the xy plane of the wire and its motion along the wire (z direction) is modulated by the periodic potential. Therefore, the electron energy can be written as

$$\varepsilon(\mathbf{k}) = \varepsilon_{\mathrm{SL}}(k_z) + \varepsilon_{mn} , \tag{2}$$

where $\varepsilon_{\mathrm{SL}}(k_z)$ is the energy dispersion along the z axis (SI denotes superlattice) and ε_{mn} is the quantized energy in the quantum-wire cross section (xy plane). We assume an infinite square-well potential in the xy plane. The energy resulting from the confinement in this plane is written as

$$\varepsilon_{mn} = \frac{(\pi\hbar)^2}{2m_{\mathrm{eff}}L^2}(m^2+n^2) \quad m,n = 1,2,\ldots \tag{3}$$

where m and n are indices assigned to the minibands split by the confinement, m_{eff} is the effective mass, and L is the width of the square well. The energy dispersion along the z direction and the miniband width are calculated by a Kronig-Penney model.[8] The periodic potential is set so that the upper miniband folded at the Brillouin-zone edge [see Fig. 1(b)] is located high enough to neglect the electron distribution even at high temperatures. In the present model, we restrict our analysis on interminiband scattering to the first four minibands that we refer to the index (m,n) being (1,1), (1,2), (2,1), and (2,2) since for the confinement and potential period considered here most of the electrons populate in the lowest miniband. For the sake of simplicity in forthcoming calculations the miniband structure is approximated by cosine shape,

$$\varepsilon_{\mathrm{SL}}(k_z) = \frac{\varepsilon_b}{2}(1-\cos k_z d_{\mathrm{SL}}) , \tag{4}$$

where ε_b is the miniband width, and d_{SL} is periodicity of the potential. Then, the density of states (DOS) is expressed as

$$D(\varepsilon) = \sum_{m,n}\{\pi d_{\mathrm{SL}}\sqrt{(\varepsilon-\varepsilon_{mn})(\varepsilon_{mn}+\varepsilon_b-\varepsilon)}\}^{-1} . \tag{5}$$

This indicates that the DOS has singular points at the top ($\varepsilon = \varepsilon_{mn}+\varepsilon_b$) and the bottom ($\varepsilon = \varepsilon_{mn}$) of each miniband as shown in Fig. 1(b).

The wave function can be written as

$$\psi(\mathbf{k},\mathbf{r}) = \zeta(k_z,z)\Lambda_{mn}(x,y) , \tag{6}$$

where

$$\Lambda_{mn}(x,y) = \frac{2}{L}\sin\frac{m\pi}{L}x \sin\frac{n\pi}{L}y . \tag{7}$$

$\zeta(k_z,z)$ is Bloch function expressed by using the nearly free-electron model[9] as

$$\zeta(k_z,z) = \left[\sum_G C_G(k_z,z)e^{iGz}\right]e^{ik_z z} = C_{\mathrm{NFE}}(k_z,z)e^{ik_z z} , \tag{8}$$

where $G = N2\pi/d_{\mathrm{SL}}$ ($N = 0, \pm1, \pm2\ldots$). We take the simplest case $N = 0$ and -1 with $C_{\mathrm{NFE}}(k_z,z)$ expressed as

$$C_{\mathrm{NFE}}(k_z,z) = \frac{1}{\sqrt{d_{\mathrm{SL}}\cosh 2\rho}}e^{-i\gamma z/2}\cos\left[\frac{\gamma}{2}z - i\rho\right] . \tag{9}$$

Here, $\gamma = 2\pi/d_{\mathrm{SL}}$, $\rho = \frac{1}{2}\ln(\sqrt{1+\Delta\kappa^2}+\Delta\kappa)$, $\Delta\kappa = (\hbar^2/2m_{\mathrm{eff}}U)[k_z^2-(k_z-\gamma)^2]$, and U is the potential barrier height.

At temperatures above 100 K, polar optical-phonon (POP) and deformation-potential (DP) acoustic-phonon scattering are dominant in III-V compound materials. Here, we make the usual assumptions that the POP energy has no dispersion and is given by the bulk phonon energy $\hbar\omega_{\mathrm{POP}} = 36$ meV, while DP scattering has a linear q_z dependence. The latter assumption is essential to account for dissipation of the electron energy when the POP scattering is completely inhibited. To avoid complexity, confined and interface phonon modes are not taken into account, since the model and its interaction Hamiltonians are still under argument. However, it is justified to use the bulk model when the QB size is larger than 100 Å,[10] or the content of Al in the $Al_xGa_{1-x}As$ barrier is small. This point will be discussed in detail later.

Ionized impurity scattering is neglected since we can practically eliminate it by introducing a modulation doping technique into an edge–quantum-wire-like structure.[1,11] Interface roughness (IF) scattering[12] is also an important process in QMS. Its effect depends strongly on the height and lateral correlation length of the interface roughness, as briefly described in Sec. III. In the main body of the text, however, we neglect IFR scattering assuming an ideal case in which uniform boxes are periodically coupled with a negligible fluctuation. Another important scattering process in the SL structure which we did not take into account is the Umklapp process in which phonons with large wave-vector scatter carriers from one minizone to the others. Although it leads to an underestimate of the scattering rates, we did not take account of this process because of the limitation of computer memories.

III. SCATTERING MODEL

In this section we derive the expression for the transition probability of the DP and POP scattering in the case of $C_{\mathrm{NFE}}(k_z,z) = 1$. Following the expression in Ref. 13, the scattering probability can be written as

$$P_j^{\pm}(\mathbf{k},\mathbf{k}')=\frac{2\pi}{\hbar}\sum_{\mathbf{q}}\frac{C_j^2}{V}F_j(\mathbf{q})|\langle\mathbf{k}'|e^{i\mathbf{q}\cdot\mathbf{r}}|\mathbf{k}\rangle|^2 \times\delta\{\varepsilon(\mathbf{k}')-[\varepsilon(\mathbf{k})\pm\hbar\omega_j]\} \quad j=\mathrm{DP},\ \mathrm{POP}$$

$$=\frac{C_j^2}{2\pi\hbar}I_j^{\pm}(\mathbf{k},\mathbf{k}')\delta\{\varepsilon(\mathbf{k}')-[\varepsilon(\mathbf{k})\pm\hbar\omega_j]\}\ , \tag{10}$$

where

$$I_j^{\pm}(\mathbf{k},\mathbf{k}')=\int d\mathbf{Q}F_j(\mathbf{Q},|k_z'-k_z|) \times\left|\int d\mathbf{R}\Lambda_{m'n'}^{*}(\mathbf{R})\Lambda_{mn}(\mathbf{R})e^{i(\mathbf{Q}\cdot\mathbf{R})}\right|^2 . \tag{11}$$

Here, $\mathbf{Q}=(q_x,q_y)$, $\mathbf{R}=(x,y)$, V is the volume of the system, and $\hbar\omega_j$ is the phonon energy with the signs of absorption (+) and emission (−). C_{DP} and C_{POP} are constant values expressed as Eq. (7) in Ref. 13. $F(\mathbf{q})$ is defined as 1 and $n_{\mathbf{q}}^{\pm}/q^2$ ($n_{\mathbf{q}}^{\pm}$ is phonon occupation number) for DP and POP scattering, respectively. Using Eq. (7), the sum of the scattering rates with arbitrary function $\phi(\mathbf{k})$ can be written as

$$\sum_{\mathbf{k}'}\phi(\mathbf{k}')P_j^{\pm}(\mathbf{k},\mathbf{k}')=\frac{L_z}{2\pi}\sum_{m'n'\pm}\int dk_z'\phi(\mathbf{k}')P_j^{\pm}(\mathbf{k},\mathbf{k}') =\frac{C_j^2}{4\pi^2\hbar}\sum_{m'n'\pm k_i}\sum\alpha(k_i)I_j^{\pm} \times\phi(m'n'k_i)\ , \tag{12}$$

where k_i is one of the solutions of $\varepsilon(\mathbf{k}')-[\varepsilon(\mathbf{k})\pm\hbar\omega_j]=0$. The coefficient $\alpha(k_i)$ is derived from integration of the energy-conservation term and is written as

$$\alpha(k_i)=\left[\frac{\varepsilon_b}{2}d_{\mathrm{SL}}|\sin k_i d_{\mathrm{SL}}|\right]^{-1} . \tag{13}$$

$I_j^{\pm}$ can be written as[14]

$$I_{\mathrm{DP}}=\frac{4\pi^2}{L^2}(1+\tfrac{1}{2}\delta_{mm'})(1+\tfrac{1}{2}\delta_{nn'}) \tag{14}$$

and

$$I_{\mathrm{POP}}^{\pm}=\frac{n_{\mathbf{q}}^{\pm}}{(2\pi)^2}\int\int d\sigma_x d\sigma_y\frac{|\Gamma_{mm'}(\sigma_x)|^2|\Gamma_{nn'}(\sigma_y)|^2}{\sigma_x^2+\sigma_y^2+\left[\frac{L}{\pi}|k_i-k_z|\right]^2} , \tag{15}$$

where

$$|\Gamma_{mm'}(\sigma)|^2=\begin{cases}4\pi^2\ , & \sigma=0,m'=m\ ,\\ \pi^2\ , & \sigma=\pm m'\pm m\ ,\\ \dfrac{1}{2}\dfrac{(16m'm\sigma)^2\{1-(-1)^{m+m'}\cos\sigma\pi\}}{\{\sigma^2-(m'+m)^2\}^2\{\sigma^2-(m'-m)^2\}^2}\ , & \text{otherwise;}\end{cases} \tag{16}$$

for DP and POP scattering, respectively. These expressions are easily expanded when $C_{\mathrm{NFE}}(k_z,z)$ is expressed as Eq. (9).

In Fig. 2(a) we show the total scattering rate $\tau(\mathbf{k})^{-1}=\sum_{\mathbf{k}',\pm}P_j^{\pm}(\mathbf{k},\mathbf{k}')$ for the case where $\varepsilon_b=30$ meV, $d_{\mathrm{SL}}=90$ Å, and $L=200$ Å. The intraminiband POP scattering does not occur in this case since the optical-phonon energy $\hbar\omega_{\mathrm{POP}}$ (=36 meV) exceeds the miniband width. The short-dashed and long-dashed lines denote the scattering rates for DP and POP scattering, respectively. The solid line indicates the sum of the scattering rate for DP and POP scattering. We set the zero energy at the bottom of the (1,1) miniband. The lateral confinement L results in an energy separation $\Delta\varepsilon_{12}=42$ meV between the bottoms of (1,1) and (1,2) minibands. The energy range spanned by the miniband is indicated by horizontal arrows.

The scattering rate is zero between 30 meV [top of the (1,1) miniband] and 42 meV [bottom of the (1,2) miniband] since there is a real minigap with no electronic states in this energy range. This minigap also causes the suppression of interminiband POP scattering for electrons in the bottom of the (1,1) miniband (hatched area). This is because electrons cannot reach the (1,2) miniband by absorbing a POP. Only DP scattering is active over this energy range. As lateral confinement increases, the energy range in which POP scattering is suppressed becomes wider, and finally, complete suppression of POP scattering is achieved when Eq. (1) is satisfied.

The feature of the DP scattering is quite similar to that of the DOS since acoustic-phonon scattering is regarded as a quasielastic process at small q_z. In Fig. 2(a) the separation between the singular points of the miniband edges reflects the q_z dependence of the phonon energy. Note that the DP scattering rate is nearly 10^{12} sec^{-1} which is still smaller than the POP rate, but much larger than the bulk value. This is due to large form factor resulting from strong confinement. The importance of the DP scattering will be emphasized in Sec. V.

Figure 2(b) shows the total scattering rate for $\varepsilon_b=60$ meV ($>\hbar\omega_{\mathrm{POP}}$), $d_{\mathrm{SL}}=90$ Å, and $L=200$ Å where intraminiband POP scattering occurs for electron energy greater than 36 meV. Most of the electrons which have accelerated to this energy easily emit an optic phonon and relax to lower energy. Moreover, the presence of several peaks caused by the interminiband POP scatter-

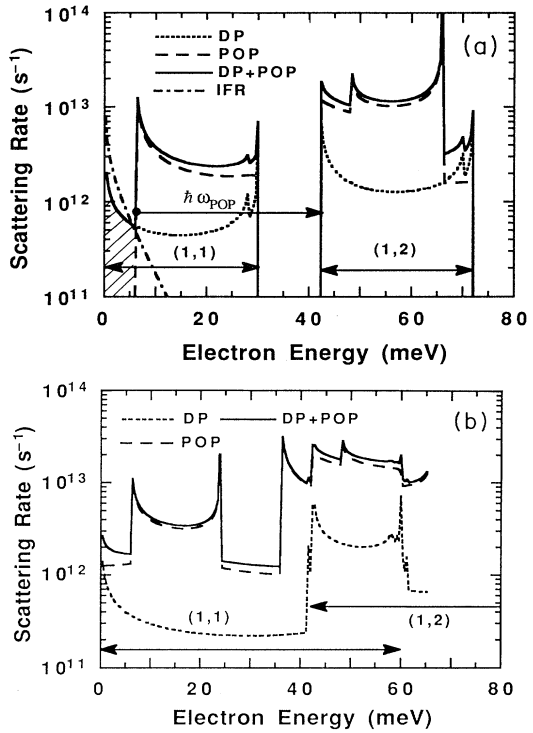

FIG. 2. Calculated scattering rates of electrons in 1D-CQB's for (a) $\varepsilon_b=30$ meV and (b) $\varepsilon_b=60$ meV. Here, $L=200$ Å, $d_{SL}=90$ Å, and $T_L=300$ K. Short-dashed, long-dashed, and solid lines denote the scattering rates for DP, POP, and the sum of these two processes, respectively. The arrows indicate the miniband width.

ing prohibit electrons from moving away to higher energy, suggesting that the coherent electron transfer by high electric field may be impossible for this structure configuration as will be discussed later.

Here, we briefly estimate the scattering rate caused by interface roughness along the wire direction. By applying a Gaussian-type autocorrelation function,[12] we obtain the scattering rate without screening as

$$1/\tau_{IFR}(k_z)=\frac{32\hbar^3\pi^4\sqrt{\pi}\Lambda\Delta^2}{m^{*2}L^6\varepsilon_b d_{SL}|\sin k_z d_{SL}|}\exp(-k_z^2\Lambda^2)\ , \quad (17)$$

where Δ is the amplitude and Λ is the lateral correlation length of the roughness. In Fig. 2(a) we plot $1/\tau_{IFR}$ for the (1,1) miniband taking $\Delta=5$ Å and $\Lambda=150$ Å, that is, a 5% fluctuation of the wire width. For very small energy, $1/\tau_{IFR}$ is comparable to the DP scattering rate, and it decreases rapidly as the electron energy increases. Therefore, IFR scattering is not important for these parameters as long as we consider the transport under high electric field. In a steady-state low-field analysis, IFR scattering ($\propto L^{-6}$) cannot be neglected especially when the wire width L decreases. However, we do not take account of this effect since it will become sufficiently small as the processing technology gets refined, while phonon scatterings remain as an unavoidable process.

IV. TRANSPORT MODEL

In studying transport phenomena at high temperatures, we cannot employ the relaxation time approximation because of strong inelastic scattering processes such as POP scattering. Therefore, we directly solve the semiclassical time-dependent Boltzmann transport equation (BTE),[15]

$$\frac{df}{dt}+\frac{eF}{\hbar}\frac{\partial f}{\partial k_z}=\left[\frac{\partial f}{\partial t}\right]_{coll}\ , \quad (18)$$

where

$$\left[\frac{\partial f(\mathbf{k})}{\partial t}\right]_{coll}=\sum_{\mathbf{k}'}\{[1-f(\mathbf{k})]f(\mathbf{k}')P(\mathbf{k}',\mathbf{k})-[1-f(\mathbf{k}')]f(\mathbf{k})P(\mathbf{k},\mathbf{k}')\}\ . \quad (19)$$

Here, $f(\mathbf{k})$ is the electron distribution function, and $P(\mathbf{k},\mathbf{k}')$ is the scattering probability from the state with wave vector $\mathbf{k}$ to the final state with $\mathbf{k}'$ and calculated in Eq. (10). F is the applied electric field and the other symbols have their usual meanings.

One popular method to solve Eq. (18) is the Monte Carlo method[16] which simulates numerically the stochastic processes of electron interaction with lattice vibrations and crystal defects. Although a recent Monte Carlo simulation of electron transport in quantum wires[17] has been shown to be very powerful for the high-field effect, memory requirement and running time for computers are quite severe to study the structural dependence of transport in 1D-CQB structures. Therefore, we employed the iterative method formulated by Rees.[18]

Because of the singularities in the DOS at the miniband edges of 1D-CQB shown in Fig. 1(b), numerical differentiation of the distribution function on the left-hand side of Eq. (18) must be handled with care because it might give an unstable solution. Therefore, we transformed Eq. (18) into the equivalent integral equation

$$f_{n+1}(k_z)=\int_0^\infty g_n(k_z-eFt'/\hbar)e^{-\Phi t'}dt'\ , \quad (20)$$

where

$$g_n(k_z)=\left[\frac{\partial f_n(k_z)}{\partial t}\right]_{coll}+\Phi f_n(k_z)\ . \quad (21)$$

Here, we introduce a self-scattering process expressed as $\Phi f_n(k_z)$, which adds no influence to the original equation. Starting from the initial distribution function f_0, we can obtain the $(n+1)$th iterative solution f_{n+1} from the nth approximate solution of Eqs. (20) and (21) by introducing f_n into the right-hand side of Eq. (20). A steady-state solution is obtained when the iterative process converges. Within this scheme, the self-scattering constant Φ determines the convergence rate of the solution. Moreover, Rees[18] showed that when Φ is chosen to be large enough, each iterative step corresponds to the time evolution of the distribution function with time step $1/\Phi$. Thus, we can obtain both steady- and transient-state distribution functions simultaneously by solving Eqs. (20) and (21) and using Eqs. (10)–(16). First, we obtain the

scattering probability and store them into memories as a lookup table. Next the iterative procedure is carried out using the lookup table. Finally the distribution function is used to calculate the electron velocity and mobility.

V. RESULTS AND DISCUSSION

A. Time-dependent solutions

In this section we show the distribution function obtained from the time-evolution analysis by solving the Boltzmann equation iteratively. In Figs. 3(a) and 3(b), we show the time variation of the distribution function at a low electric field ($F=100$ V/cm) and its deviation from the initial Maxwell distribution function. Here, we use the same parameters as in Fig. 2(a) where optical-phonon scattering is partially suppressed around the bottom of the first miniband. The horizontal axis denotes the wave vector along the k_z direction normalized to half of the reciprocal lattice vector of the SL. The iterative procedure was performed at $1/\Phi=20$ fsec, and the solutions were picked up at every 0.4 psec.

The feature of the nonequilibrium distribution function is clearly different from the displaced Maxwellian shown in dashed line in Fig. 3(a). Here, the displacement $\Delta k_x = eF\tau/\hbar$ is given by setting the relaxation time $\tau=2$ psec and $F=100$ V/cm. After a few picoseconds the distribution function shows two shoulders at $k_z=\pm 0.3\pi/d_{\rm SL}$ and a rapid decrease at the origin of the minizone. The shoulders correspond to the peak in the scattering rate at 6 meV above the first miniband edge shown in Fig. 3(a), and which is due to the scattering by POP absorption to the bottom of the second miniband. Therefore, electrons with wave vector $|k_z|<0.3\pi/d_{\rm SL}$ are easily accelerated since they suffer neither POP absorption nor POP emission, which results in a depletion of carriers around the origin. Above $0.3\pi/d_{\rm SL}$, inter-miniband scattering with carrier exchange between the minibands occurs quite often, resulting in a small shift from the initial distribution. Thus, the abrupt change in the scattering rate causes a nonuniform deformation of the electron distribution, and accumulation of electrons at energies where the scattering rate has singularities [see Fig. 3(b)]. A similar behavior has recently been obtained in quantum-wire structures.[19]

Another important difference in the displaced Maxwellian is an increase of the electron distribution in the negative k_z region. This effect is caused by the reflection of electrons at the minizone edge due to the periodicity of

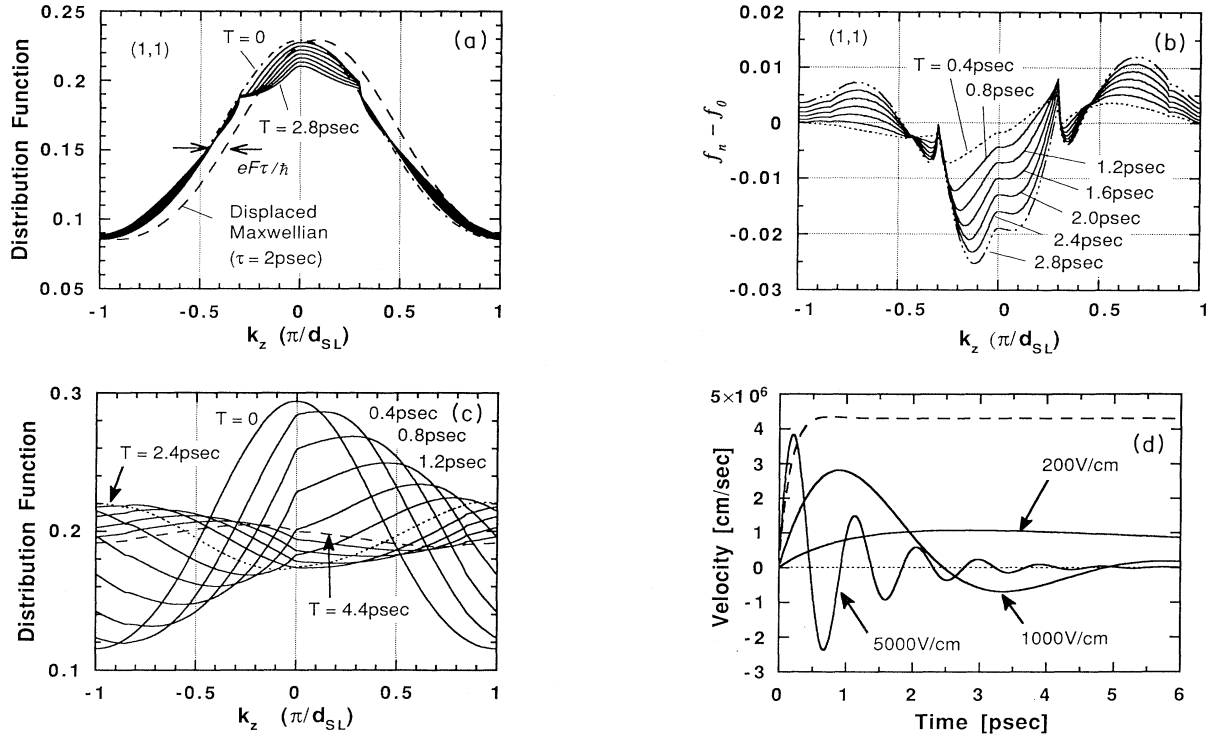

FIG. 3. (a) Time evolution of the distribution function f_n and (b) the difference between f_n and the Maxwellian distribution function f_0. The parameters used here are $\varepsilon_b=30$ meV, $L=200$ Å, and $F=100$ V/cm. The results are picked up at every 0.4 psec. The horizontal axis denotes the wave vector along the z direction normalized by half of the minizone period. (c) Time evolution of the distribution under a high electric field. Here, $\varepsilon_b=30$ meV, $L=150$ Å, and $F=1000$ V/cm. Short-dashed and long-dashed lines denote the distribution at $T=2.4$ and 4.4 psec, respectively. (d) Electron velocity for three different electric fields ($F=200$, 1000, and 5000 V/cm) as functions of time. The parameters for solid lines are the same as in Fig. 3(c) except for the electric field. The dashed line is for $\varepsilon_b=60$ meV, $L=200$ Å, and $F=1000$ V/cm. Other parameters used in (a)–(d) are $T_L=300$ K, $d_{\rm SL}=90$ Å, $N_d=5\times10^5$ cm^{-1}, and $1/\Phi=20$ fsec.

the 1D-CQB structure. Since the electrons reflected to the other zone boundary tend to have negative velocity, the net current decreases correlatively. Thus, the periodicity introduced in the 1D system which causes the formation of minibands has somewhat of a negative effect on the transport properties.

In Fig. 3(c), we show the time evolution of the distribution function under the condition where POP scattering is suppressed. Here, $d_{SL}=90$ Å, $N_d=5\times10^5$ cm^{-1}, $L=150$ Å, $F=10^3$ V/cm, and $1/\Phi=20$ fsec. The initial distribution function is Maxwellian and the data were picked up after every 0.4 psec. The figure shows the electron acceleration by the high electric field with a time shift of the center of the distribution function accompanied by a broadening. After 2.4 psec, the center of the distribution function is reflected to the opposite zone boundary because of the periodicity of the mini-Brillouin zone. Note also that as time goes on, the distribution function at the miniband edges becomes comparable with that at the zone center. This indicates that the distribution function tends to spread out over all the miniband width which is quite different from a displaced Maxwellian distribution. Another important feature of the carrier dynamics in the miniband structure is seen after 0.8 psec when many electrons are accelerated to the negative mass region which induces a drop in the electron velocity.

In Fig. 3(d) we show the variation of the drift velocity $\langle v\rangle=\sum v(\mathbf{k})f(\mathbf{k})/\sum f(\mathbf{k})$ as a function of time for three values of the electric field. The conditions for the solid lines are the same as Fig. 3(c). Bloch oscillations are clearly seen with the frequency $2\pi\hbar/eFd_{SL}$. The damping of the oscillations is due to a degradation of the coherence of the electron distribution, i.e., the electrons are not reflected simultaneously at the minizone edges, which tends to spread out the distribution over all the mini-Brillouin zone. This is the reason why the final velocity at the convergence shows almost zero value.

On the other hand, when the POP scattering is not suppressed, Bloch oscillations cannot be seen even at $F=10^3$ V/cm because of the high scattering probabilities. The dashed line in Fig. 3(d) shows the electron velocity for the case of $\varepsilon_b=60$ meV, $L=200$ Å, $d_{SL}=90$ Å, $N_d=5\times10^5$ cm^{-1}, $F=10^3$ V/cm, $T_L=300$ K, and $1/\Phi=20$ fsec, in which both interminiband and intraminiband POP scattering processes are present. The velocity converges to a constant value before reaching the negative mass region since frequent absorption and emission processes of optic phonons lead to efficient randomization of carriers with different energies and prohibit the coherent carrier transport. From these results we conclude that negative velocity and Bloch oscillations may be realized even at room temperature as long as the condition for quenching of POP scattering is satisfied.

B. Steady-state solutions

Next we discuss the steady-state analysis under low electric fields. In Fig. 4(a), we show the low-field mobility calculated as functions of the cross-sectional width L of the wire. The squares and solid circles correspond to the mobility for the case of a wide miniband ($\varepsilon_b=60$ meV)

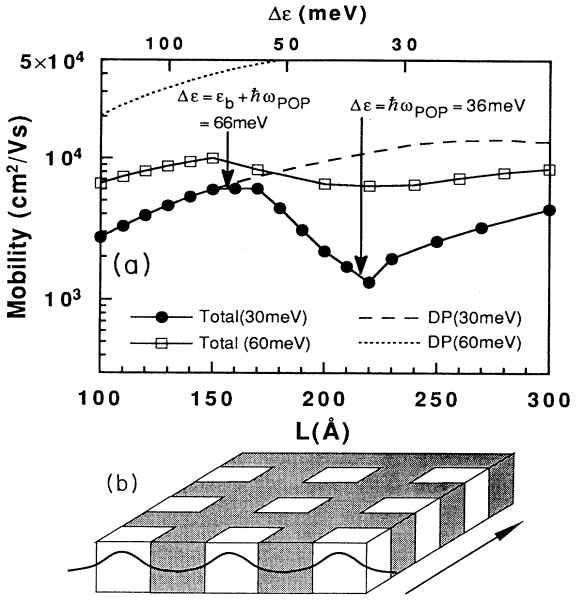

FIG. 4. (a) Calculated mobility at $T_L=300$ K as a function of the cross-sectional width L of the wire. Squares and solid circles denote the total mobility for $\varepsilon_b=60$ and 30 meV, respectively. Dotted and dashed lines indicate the mobility determined by DP scattering. Here, $d_{SL}=90$ Å, $N_d=5\times10^5$ cm^{-1}, $F=100$ V/cm, and $T_L=300$ K. (b) Schematic illustration of 2D-CQB's.

and a narrow miniband (30 meV), respectively. Dashed and dotted lines indicate the mobility component for these two cases that would be determined by the DP scattering only. Here, we set $d_{SL}=90$ Å, $N_d=5\times10^5$ cm^{-1}, and $F=100$ V/cm. The upper horizontal scale denotes the energy generation $\Delta\varepsilon=\varepsilon_{12}-\varepsilon_{11}$.

In the case of $\varepsilon_b=30$ meV where the intraminiband POP scattering is suppressed, the minigap width $\varepsilon_g=\Delta\varepsilon-\varepsilon_b$ is larger than $\hbar\omega_{POP}$ as long as L is smaller than 159 Å. Therefore, the total mobility for $L<159$ Å is not affected by POP scattering, but is mainly determined by DP scattering. When L is set larger than 159 Å, the POP contribution comes in. Indeed, when $L=200$ Å, the large dip of the mobility appears. This is caused by optic-phonon resonance between the two minibands and resembles to the well-known magnetophonon resonance[20] whose band separation originates from the Landau splitting. The POP scattering is strongly enhanced when the optic-phonon energy equals the energy separation $\Delta\varepsilon$ between the bottoms of the minibands where due to the singularities, the joint DOS is maximum. The rapid recovery of the mobility with decrease of L indicates the effective reduction of the POP scattering.

Although the mobility feature clearly shows the effect of suppression of POP scattering, the mobility amplitude itself is not large as compared to the bulk value ($\mu=6000$ cm^2/V s at 300 K) or other QMS structures. Three factors limit the mobility to low values: first, the acoustic-phonon scattering is enhanced by the strong confinement (size effect[21]) in the wire which brings its contribution to the level comparable to the POP scattering rate. The

second factor is the miniband structure itself; in order to suppress intraminiband POP scattering, one needs to choose a narrow miniband. This, in turn, causes an increase of the effective mass by a factor of 3 to 4 times larger than the bulk value at the Γ point and reduces the mobilities. This explains why the mobility for the case of $\varepsilon_b = 60$ meV is larger than that of $\varepsilon_b = 30$ meV. Moreover, the effect of a negative mass region in the upper part of the miniband also decelerates the electron motion. The third factor is Bragg reflection at the minizone edges; once electrons reach the minizone boundaries, electrons are reflected back to the opposite zone boundaries with negative wave vector. Therefore, these shifts in the electron distribution by the electric field result in a total loss in the total momentum.

To achieve the highest mobility, one must optimize the structure parameters L, ε_b, and d_{SL} which influence these three factors. However, the highest value of the mobility is always limited by the POP scattering except in the case where POP scattering is completely suppressed as discussed earlier. Therefore, reducing the acoustic-phonon scattering is the most important challenge to improve the mobility under the suppression of POP scattering.

Among the three mobility limiting factors discussed above, the second and third ones cannot be avoided since they derive from the essential characteristics of the miniband. However, the first factor, or the confinement-induced enhancement of DP scattering can be reduced if one employs 2D- or 3D-CQB's (super crystals) as shown in Fig. 4(b). Since the confinement in these structures is weaker than in the 1D case, the electron-phonon interaction can, in principle, be reduced. The band structure is almost the same as 1D case except that new minibands are formed along the other directions. In addition, the energy separation between the upper minibands is still maintained, or in some cases can become larger since the resulting minigap can be far larger than the energy separation between quantized levels. The details of the analysis of 2D- and 3D-CQB's will be discussed in a forthcoming publication.

Before concluding, we would like to point out two important considerations which have been omitted in the present model. One is the broadening of the DOS caused by scattering and roughness of the interface.[22] The broadening removes the singularities in the DOS which play quite an important role in the determination of the distribution function. Moreover, since band tailing resulting from the DOS broadening may appear in the minigap, residual optical-phonon scattering may still be active even when $\varepsilon_g > \hbar\omega_{\mathrm{POP}}$.

Another important effect is the consideration of confined and interface phonon modes.[23] When the well width d_W decreases below 40 Å, the nature of dominant phonon modes is affected by confinement. The acoustic-phonon branch is folded at $q = \pi/d_{\mathrm{SL}}$ generating many new phonon modes around $q = 0$. The optical-phonon branches split to several discrete energy levels with no dispersion (confined phonon modes) and localized modes at the heterointerfaces (interface phonon modes). These effects change the electron-phonon interaction Hamiltonian as well as the energy exchange involved during the interaction. However, these effects will not qualitatively change our conclusions as long as GaAs-like POP modes are concerned. This is because the whole set of GaAs-like modes affected by the confinement have almost the same energy (between $\hbar\omega_{\mathrm{TO}} = 33.3$ meV and $\hbar\omega_{\mathrm{LO}} = 36$ meV) and almost the same consequences as bulk phonons.[24] Thus, the condition of suppression of optical-phonon scattering [Eq. (1)] is still maintained. Note that AlAs-like interface phonon modes become important with decreasing the well width.[25] Since they have higher energy than that of GaAs-like modes, the condition, Eq. (1), has to be changed to realize complete suppression of POP scattering.

VI. CONCLUDING REMARKS

We have presented a transport analysis in 1D-CQB structures at room temperature by using an iterative technique applied to the time-dependent Boltzmann equation. Transient solutions of the distribution function predict the occurrence of Bloch oscillations in the picosecond regime. In the steady-state analysis, the mobility in 1D-CQB's is shown to depend strongly on wire sizes and periodicity. The important requirement to realize long-lasting Bloch oscillations and high-mobility systems at high temperatures is to set up the condition in which DP scattering in CQB systems is also suppressed. We believe that this requirement can be satisfied by manipulating the miniband structures, including the possible use of 2D and 3D coupled quantum-box structures.

ACKNOWLEDGMENTS

One of us (J.P.L.) would like to acknowledge partial support from ARO under Grant No. DAAL 03-91-G-0052. J.P.L. is also indebted to Hitachi LTD for supporting his research work during his stay at RCAST. This work is partly supported by a Grant-in-Aid for Scientific Research from the Ministry of Education, Science and Culture, and also partly by the JRDC through the ERATO quantum wave project.

*Permanent address: Beckman Institute for Advanced Science and Technology, University of Illinois, 405 North Mathes Avenue, Urbana, IL 61801.

[1] H. Sakaki, Jpn. J. Appl. Phys. **12**, L735 (1980).

[2] Y. Arakawa and H. Sakaki, Appl. Phys. Lett. **40**, 939 (1982).

[3] H. Sakaki, Jpn. J. Appl. Phys. **28**, L314 (1989).

[4] S. Datta, M. R. Melloh, S. Bandyopadhyay, and R. Noren, Phys. Rev. Lett. **55**, 2344 (1985); B. J. van Wees, L. P. Kowenhoven, C. J. P. M. Harmans, J. G. Williamson, C. E. Timmering, M. E. I. Broekaart, C. T. Foxon, and J. J. Haris, *ibid.* **62**, 2523 (1989).

[5] L. P. Kouwenhoven, A. T. Johnson, N. C. van der Vaart, and C. J. P. M. Harmans, Phys. Rev. Lett. **67**, 1626 (1991).

[6] S. Tsukamoto, Y. Nagamune, M. Nishioka, and Y. Arakawa, J. Appl. Phys. **71**, 533 (1992); S. Tsukamoto *et al.*, in *The Proceedings of the 19th International Symposium on Gallium*

Arsenide and Related Compounds, edited by T. Ikegami, F. Hasegawa, and Y. Takeda (Karuizawa, Japan, 1992), pp. 929–932.
[7]L. Esaki and R. Tsu, IBM J. Res. Dev. **14**, 61 (1970); L. Esaki and L. L. Chang, Phys. Rev. Lett. **33**, 495 (1974).
[8]G. Bastard, Phys. Rev. B **24**, 5693 (1980).
[9]J. F. Palmier and A. Chomette, J. Phys. (Paris) **43**, 381 (1982).
[10]K. W. Kim, M. A. Stroscio, A. Bhatt, R. Mickevicius, and V. V. Mitin, J. Appl. Phys. **70**, 319 (1991).
[11]M. Tsuchiya, H. Sugawara, T. Inoshita, A. Shimizu, and H. Sakaki, Surf. Sci. **267**, 296 (1992).
[12]J. Motohisa and H. Sakaki, Appl. Phys. Lett. **60**, 1315 (1992).
[13]G. Fishman, Phys. Rev. B **36**, 7488 (1987).
[14]V. K. Arora and F. G. Awad, Phys. Rev. B **23**, 5570 (1981).
[15]D. L. Rode, *Semiconductors and Semimetals* (Academic, New York, 1975), Vol. 10, Chap. 1.
[16]C. Jacoboni and L. Reggiani, Rev. Mod. Phys. **55**, 645 (1983).
[17]S. Briggs and J. P. Leburton, Phys. Rev. B **38**, 8163 (1988); Phys. Rev. **43**, 4785 (1991).
[18]H. D. Rees, J. Phys. Chem. Solids **30**, 643 (1969); J. Phys. C **5**, 641 (1972).
[19]J. P. Leburton, Phys. Rev. B **45**, 11 022 (1992).
[20]H. Noguchi, T. Takamasu, N. Miura, and H. Sakaki, Phys. Rev. B **45**, 12 148 (1992).
[21]J. P. Leburton, Appl. Phys. Lett. **56**, 2850 (1984).
[22]J. P. G. Taylor, K. J. Hugill, D. D. Vvedensky, and A. MacKinnon, Phys. Rev. Lett. **67**, 2359 (1991).
[23]M. V. Klein, IEEE J. Quantum Electron. **QE-22**, 1760 (1986); G. Fasol, M. Tanaka, H. Sakaki, and Y. Horikoshi, Phys. Rev. B **38**, 6056 (1988); N. Mori and T. Ando, Phys. Rev. **40**, 6175 (1989); D. J. Mowbray, M. Cardona, and K. Ploog, Phys. Rev. B **43**, 1598 (1991).
[24]T. Tsuchiya and T. Ando, Semicond. Sci. Technol. **7**, B73 (1992).
[25]H. Noguchi, T. Takamasu, N. Miura, J. P. Leburton, and H. Sakaki, in *Phonons in Semiconductor Nanostructures,* NATO Advanced Research Workshop, edited by J. P. Leburton, J. Pascual, and C. Sotomayor Torres (Kluwer Academic, Boston, in press).